Plasma electron fluid motion and wave breaking near a density transition

R. J. England, J. B. Rosenzweig, and N. Barov
Department of Physics and Astronomy, University of California Los Angeles, Los Angeles, California 90095
(Received 11 January 2002; revised manuscript received 12 April 2002; published 25 July 2002)

Recently, Suk, Barov, and Rosenzweig [Phys. Rev. Lett. **86**, 1011 (2001)] proposed a scheme for trapping background electrons in a plasma wake field using a sudden downward transition in the background ion density, where the density transition length is small compared to the plasma skin depth. In the present paper we present a fluid dynamical description of this mechanism that is self-consistent up to the point of wave breaking. A one-dimensional nonlinear relativistic second-order differential equation is derived for the electron fluid velocity in Lagrangian coordinates. Numerical integrations of this equation are used to map out the regions of parameter space in which wave breaking occurs and to determine the extent of the downstream region of plasma involved in wave breaking. Comparisons with one-dimensional particle-in-cell (PIC) simulations show that the onset of trapping occurs at the parameter values where wave breaking begins in the fluid analysis, but that the downstream extent of plasma involved in wave breaking is not a reliable predictor of the number of trapped particles. The PIC simulations also reveal that particles initially located on the upstream side of the density transition may become trapped, although these particles do not participate in wave breaking in the fluid description.

DOI: 10.1103/PhysRevE.66.016501 PACS number(s): 29.17.+w, 29.27.−a, 52.40.Mj, 52.75.Di

I. INTRODUCTION

In a recent work by Suk, Barov, and Rosenzweig [1], a scheme was proposed for trapping of background plasma electrons in a plasma wave driven by an ultrarelativistic electron beam (plasma wake-field accelerator, or PWFA) using a sharp downward plasma density transition. This effect allows for the synchronized injection of ultrashort pulses into a spatially compact accelerating wave, and it has significant simplifying advantages over previously proposed plasma injection schemes involving multiple lasers [2–5]. As a robust and straightforward method of injecting the appropriate number of electrons into the small phase space acceptance of plasma waves, this scheme has attracted the attention of the advanced accelerator community.

The physical scenario involved in this injection is summarized in Fig. 1. Suk, Barov, and Rosenzweig in a one-dimensional (1D, in z) analysis, have demonstrated that injection based on a density transition is caused by the phase mixing of plasma electrons as they are driven backwards from the lower density (II) to higher density (I) plasma region, and subsequently return to region II. As the particles are advanced in phase upon reentry into region II, they are injected into a more favorable region in phase space for trapping into the plasma wave. In order to observe this effect, it was found that the characteristic length over which the density transition occurs must be smaller than the plasma skin depth $k_p^{-1}=\nu_b/\omega_p$, where the beam velocity is indicated by ν_b and the plasma frequency is given by $\omega_p=\sqrt{4\pi n_0 e^2/m_e}$. Physically, this requirement arises because the amplitude of the moderately relativistic oscillatory electron motion in a large-amplitude relativistic plasma wave is of the approximate magnitude of k_p^{-1}. It should be noted that since advanced accelerator applications inherently involve only relativistic waves, that the plasma electron motion must be moderately relativistic in the scenario of present interest, where plasma electrons must end up trapped in a relativistic wave.

The analysis in Ref. [1] was based on one- and two-dimensional (2D, with cylindrical symmetry) simulations, and 1D theoretical work. The theoretical model developed in this work concentrated on following the single electron motion in regions I and II, using wave fields derived by assuming that the wave motion is obtained from the uniform density response in each respective region. This analysis has the advantage of illuminating the transition of plasma electrons from oscillatory to directed motion, trapped in the potential of the ultrarelativistic wave on the downstream (increasing z) side of the density transition. It is, however, a model that does not deal self-consistently with the plasma fluid motion, which is assumed to be regular on either side of the transition, with a discontinuity in the description of the fluid variables at the transition. The purpose of the present paper is to adopt the opposite emphasis, to study the fluid motion in this scheme up until wave-breaking. Our analysis illuminates the plasma fluid motion, at the expense of accurately following

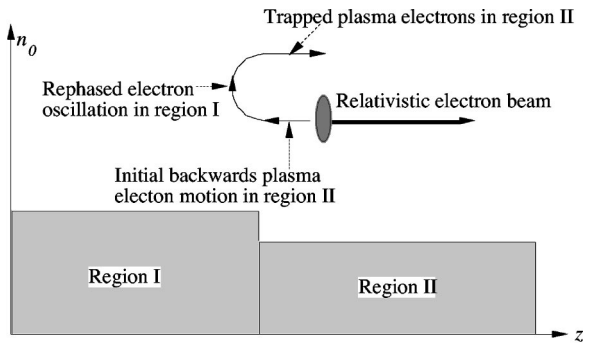

FIG. 1. Trajectory of a plasma electron (solid curve) which begins at a point in region II and is negatively accelerated into the higher-density region I by the passage of the beam. Upon returning to region II, the electron has been rephased and is trapped by the wave generated in the wake of the beam.

the motion after wave breaking, when fluid models are no longer strictly valid.

The scheme proposed in Ref. [1] assumes that the initial excitation occurs entirely within the first half of a plasma oscillation, and therefore requires a driving beam shorter than the plasma skin depth. The amplitude of the resulting excitation is determined by the density profile of the beam. Instead of assuming a particular functional form for the longitudinal profile, and thereby complicating the analysis, we simply impose as a boundary condition the transient introduction of an electric field at a position traveling with light speed in z, and then examine the plasma fluid motion in the wake of this excitation. In the example of the PWFA, this corresponds to an ultrarelativistic beam of negligible length, in which case the electric field after passage of the beam is $k_p\sigma_r \gg 1$, where σ_b is the surface charge density of the 1D bunched electron beam. In the case where the driver is an intense laser (laser wake-field accelerator, LWFA), a similar analysis could be employed, but with the initial transient force acting in the opposite direction. This scenario awaits future investigation.

The present analysis is additionally concerned with the dynamical state of the fluid electrons, so we adopt a Lagrangian description of the plasma motion, as opposed to previous works which have emphasized wave properties, and thus employed an Eulerian approach. With this Lagrangian analysis, we examine the dynamics of wave breaking and deduce where and when the wave breaking is initiated. We also examine the conditions that lead to wave breaking, examining in particular the combinations of initial E_z and relative density parameter $\eta=(n_{0,\mathrm{I}}-n_{0,\mathrm{II}})/n_{0,\mathrm{I}}$ which produce wave breaking. The results of the Eulerian analysis up until this point are exact and self-contained, but must be extended with additional tools in order to examine two topics. The first is the extent of the initial region of plasma which is involved in wave breaking, which may be estimated from our analysis. The second is the degree to which the wave breaking in the present scenario actually corresponds to trapping of the affected plasma electrons. Both of these questions will be approached by comparison of the analytical theory with 1D simulations.

II. REVIEW OF EULERIAN ANALYSIS

We begin the analysis by reviewing the equations governing plasma fluid motion in Eulerian coordinates. Maxwell's equations and the fluid electron equation of motion read

$$\frac{\partial \mathbf{p}}{\partial t}+c(\boldsymbol{\beta}\cdot\boldsymbol{\nabla})\cdot\mathbf{p}=-e(\mathbf{E}+\boldsymbol{\beta}\times\mathbf{B}),$$

$$\boldsymbol{\nabla}\cdot\mathbf{E}=4\pi e(n_0-n-n_b),$$

$$\boldsymbol{\nabla}\times\mathbf{E}=-\frac{1}{c}\frac{\partial \mathbf{B}}{\partial t}, \tag{1}$$

$$\boldsymbol{\nabla}\times\mathbf{B}=-4\pi e(n\boldsymbol{\beta}+n_b\boldsymbol{\beta}_b)+\frac{1}{c}\frac{\partial \mathbf{E}}{\partial t},$$

$$\boldsymbol{\nabla}\cdot\mathbf{B}=0,$$

where n_0, n, and n_b are the ion, electron, and beam densities, $\boldsymbol{\beta}=v/c$ and $\boldsymbol{\beta}_b=v_b/c$ are the normalized plasma electron and beam velocities, and $\mathbf{p}=\gamma m_e c\boldsymbol{\beta}$ is the relativistic plasma electron momentum. If the waves are restricted to one spatial dimension (that is, $\mathbf{E}$, $\boldsymbol{\beta}$, and n contain only z and t dependence), the plasma is unmagnetized ($\mathbf{B}=\mathbf{0}$), and the time dependence is assumed to obey the *wave ansatz* (combined z and t dependences are of the form $\phi=\omega_p t-k_p z$), then the derivatives transform according to

$$\frac{\partial}{\partial t}\rightarrow\omega_p\frac{d}{d\phi},\quad \frac{\partial}{\partial z}\rightarrow -k_p\frac{d}{d\phi}. \tag{2}$$

Equations (1) can then be brought into the form of an ordinary differential equation for the normalized longitudinal velocity β and a separate algebraic expression for n,

$$\frac{d^2}{d\phi^2}\frac{1-\beta_b\beta}{\sqrt{1-\beta^2}}=\beta_b^2\left[\frac{\beta}{\beta_b-\beta}+\frac{n_b}{n_0}\right], \tag{3}$$

$$n=\frac{n_0\beta_b}{\beta_b-\beta}. \tag{4}$$

These are the usual equations for one-dimensional plasma waves, originally obtained by Akhiezer and Polovin in 1956 [6]. The electric field may be obtained from β by way of the electron fluid equation of motion, which can be cast into the form

$$\frac{eE}{mc\omega_p}=\frac{1}{\beta_b}\frac{d}{d\phi}\frac{1-\beta_b\beta}{\sqrt{1-\beta^2}}. \tag{5}$$

For a beam of negligible length and surface charge density σ_b, the electric field discontinuity experienced by a plasma electron as the beam passes by is, as stated above, of magnitude $4\pi\sigma_b$. Since the beam density n_b is zero in the wake of the beam, and the plasma electrons are assumed to be at rest prior to the passage of the beam, Eq. (3) may be solved in homogeneous form subject to the initial conditions $\beta=0$ and $E=-4\pi\sigma_b$ evaluated at the beam position $\phi=0$, which is stationary in this Galilean frame. Under these conditions, oscillatory solutions for β may be obtained analytically from Eq. (3) in terms of elliptic integrals. The nonlinear solutions are periodic functions whose amplitude β_m is related to the maximum electric field E_m by the simple expression [6],

$$\frac{eE_m}{mc\omega_p}=\left[\frac{1}{\sqrt{1-\beta_m^2}}-1\right]^{1/2}. \tag{6}$$

Wave breaking in a plasma of uniform ion density occurs when the wave amplitude becomes sufficiently large that the peak fluid velocity β_m exceeds the wave phase speed β_b. The electric field amplitude at wave breaking is therefore obtained from Eq. (6) by setting $\beta_m=\beta_b$.

For the case of a plasma with a sudden decrease in the value of the ion density, Suk, Barov, and Rosenzweig treat the plasma responses in the regions of different ion density as being independently governed by Eq. (3) subject to the same initial conditions, but with different values for n_0. Since the electric field in either region is static in the Galilean frame moving with the wave, the interface between regions I and II, which in the frame of the wave travels in the negative z direction with speed v_b, is described as a discontinuous joining of two Hamiltonian phase spaces. The dynamics of trapping are then modeled by performing a Hamiltonian analysis on the single-particle motion of a trapped electron. But since the fluid variables in this treatment are discontinuous at the interface, a model of the trapping mechanism is obtained at the expense of a self-consistent description of the fluid dynamics.

III. LAGRANGIAN ANALYSIS

In order to formulate a self-consistent fluid dynamical description of a 1D cold plasma wave in the presence of a discontinuity in the ion density, we must derive from Eqs. (1) a set of expressions for the evolution of the fluid variables that are valid when n_0 has arbitrary spatial dependence. Since n_0 then depends on z but not on t, the *wave ansatz* [Eq. (2)] must be abandoned. In Eulerian coordinates, the result is a second-order partial differential equation for β with mixed derivatives. Transforming to Lagrangian coordinates affords us the following advantages: the transformed fluid velocity is governed by an ordinary differential equation rather than a partial differential equation; we can examine the motion of individual fluid elements; and we obtain a mathematical test for wave breaking.

We define $\xi(z_0,\tau)$ to be the position of a fluid element a time τ after it was found to be located at point z_0. The Lagrangian coordinate transformation is then implemented by making the substitutions $z\rightarrow\xi(z_0,\tau)$, $t\rightarrow\tau$. Since the functional dependences of the fluid variables are altered by the coordinate change, we denote the transformed functions by adding a tilde: $\beta(z,t)\rightarrow\tilde{\beta}(z_0,\tau)$, $n(z,t)\rightarrow\tilde{n}(z_0,\tau)$, $E(z,t)\rightarrow\tilde{E}(z_0,\tau)$. The function $\xi(z_0,\tau)$ represents the trajectory of an individual fluid element, so the convective derivative satisfies the transformation rule

$$\frac{\partial}{\partial t}+c\beta\frac{\partial}{\partial z}\rightarrow\frac{\partial}{\partial\tau}. \tag{7}$$

By combining the t and z derivatives in Eqs. (1) into convective derivatives, we can utilize the substitution above to obtain an ordinary differential equation for $\tilde{\beta}$,

$$\frac{d^2}{d\tau^2}\frac{\tilde{\beta}}{\sqrt{1-\tilde{\beta}^2}}=-\frac{4\pi e^2}{m}(\tilde{\beta}\tilde{n}_0-\tilde{\beta}\tilde{n}_b+\beta_b\tilde{n}_b). \tag{8}$$

For comparison with Eqs. (4) and (5), the fluid density and electric field in Lagrangian coordinates are given by

$$\tilde{n}=\frac{n_0}{\partial\xi/\partial z_0}, \tag{9}$$

$$\frac{e\tilde{E}}{mc}=-\frac{\partial}{\partial\tau}\frac{\tilde{\beta}}{\sqrt{1-\tilde{\beta}^2}}. \tag{10}$$

As in the Eulerian analysis, if the effect of the beam is represented by a transient excitation of the electric field, then Eq. (8) may be solved in a homogeneous form ($n_b=0$), subject to appropriate initial conditions. If we permit spatial dependence in n_0, the homogeneous form of Eq. (8) reads

$$\frac{d^2}{d\tau^2}\frac{\tilde{\beta}}{\sqrt{c^2-\tilde{\beta}^2}}=-\omega_p^2(\xi)\tilde{\beta}. \tag{11}$$

A fluid element executes relativistic oscillations subject to the local value of the plasma frequency $\omega_p(\xi)=\sqrt{4\pi n_0(\xi)e^2/m_e}$ at the instantaneous position of the fluid element. Since $c\tilde{\beta}=\partial\xi/\partial\tau$, Eq. (11) represents a third-order differential equation in the function ξ.

In transformed variables, the initial conditions corresponding to a beam of negligible length and surface charge density σ_b are $\tilde{E}=-4\pi\sigma_b$, $\tilde{\beta}=0$, and $\xi=z_0$ to be applied at time $\tau=z_0/v_b$, when the beam encounters the fluid element located at point z_0. By virtue of Eq. (10), the first of these boundary conditions is equivalent to specifying the integrated acceleration of the fluid element after it encounters the beam. For the case of an instantaneous density transition, ω_p^2 is a step function having the value $\omega_{p,\mathrm{I}}^2=4\pi e^2 n_{0,\mathrm{I}}/m_e$ in the upstream region and the value $\omega_{p,\mathrm{II}}^2=4\pi e^2 n_{0,\mathrm{II}}/m_e$ in the downstream region. The plasma oscillations are therefore characterized by a sudden change in wavelength at the interface. In this situation, a fluid element initially located just inside region II spends much of its oscillation in region I before returning to its initial position z_0 advanced in phase relative to the nominal (uniform plasma) region II oscillation. This rephasing of the plasma electrons is the mechanism for trapping found by the Hamiltonian analysis of Suk, Barov, and Rosenzweig.

Numerical integration of Eq. (11) provides solutions for $\xi(z_0,\tau)$, from which the other fluid variables may be obtained using Eqs. (9) and (10). Upon reverting back to Eulerian coordinates, we find that the functions $\beta(z,t)$ and $E(z,t)$ produced by the fluid analysis are continuous across the density interface, and are initially single-valued everywhere. However, less than one plasma oscillation after the driving beam crosses the density transition, the rephasing mechanism mentioned above causes the trajectories of the rephased fluid elements to begin intersecting, leading to multivalued fluid variables and a breaking of the plasma wave. In the region where charge sheets have crossed, $\partial\xi/\partial z_0\leqslant 0$. This mathematical condition may be equated with wave breaking by noting that, for negative $\partial\xi/\partial z_0$, Eq. (9) implies a nonphysical value for the electron density.

Figure 2 illustrates the evolution of the plasma electron momentum and density under the present fluid analysis for

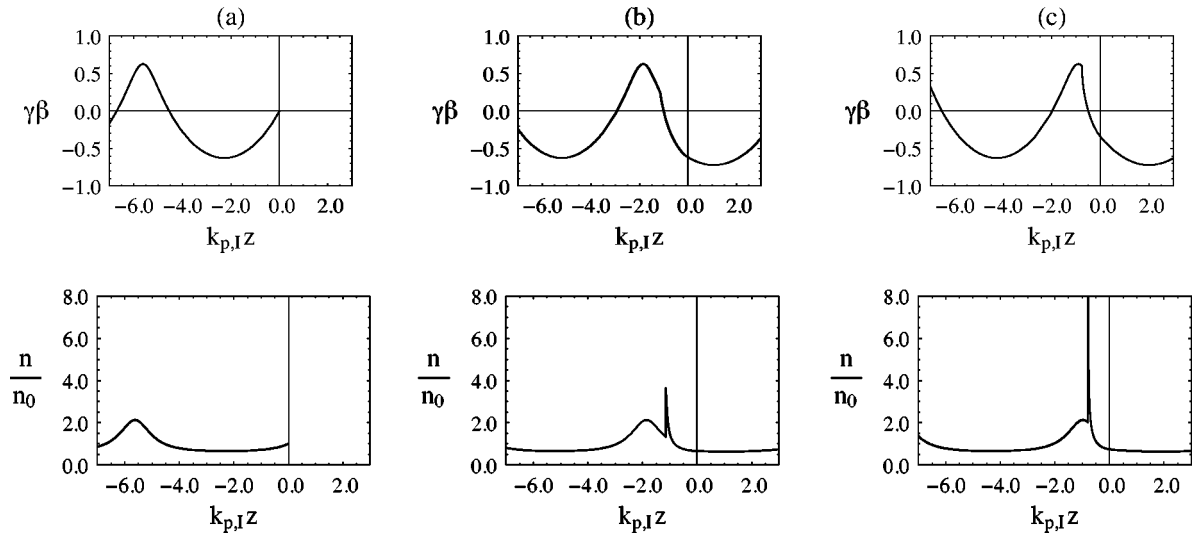

FIG. 2. Normalized plots of density and momentum at three successive times leading to wave breaking. (a) At time $t=0$, the driving beam is located at the interface ($z=0$) and the momentum and electron density have the characteristic profiles. (b) At time $t=0.6\times 2\pi/\omega_{p,\mathrm{I}}$, a sharp density spike forms. (c) At $t=0.747\times 2\pi/\omega_{p,\mathrm{I}}$ wave breaking occurs, the density spike becomes infinitely high, and the momentum acquires infinite slope near the peak.

the initial conditions $eE_m/mc\omega_{p,\mathrm{I}}=0.6$, $\beta_b=1$, and $(n_{0,\mathrm{I}}-n_{0,\mathrm{II}})/n_{0,\mathrm{I}}=0.225$. The quantities $\gamma\beta$ and n/n_0 are shown as functions of z at three successive times leading up to wave breaking, beginning at $t=0$ when the driving beam is located at the density interface. After 0.6 of a region I plasma oscillation has elapsed, a sharp density spike has formed. After 0.747 of a region I plasma oscillation, wave breaking begins, the density spike becomes infinitely high, and the fluid momentum acquires an infinite slope near the peak. A physically important clarification obtained from this analysis is that wave breaking in the Lagrangian fluid model begins in region I. This is to be contrasted with the Hamiltonian analysis of Ref. [1], in which the trapping occurs in region II following a rephasing in region I.

IV. MAPPING THE PARAMETER SPACE

Solutions for ξ are sensitive to the physical parameters of Eq. (11) and its boundary conditions, namely, E_m, β_b, and the relative change in ion density $\eta=(n_{0,\mathrm{I}}-n_{0,\mathrm{II}})/n_{0,\mathrm{I}}$. The condition $\partial\xi/\partial z_0\leqslant 0$ provides a simple mathematical test for wave breaking, which may be used to determine: (1) the values of the parameters that are conducive to wave breaking, and (2) the downstream extent of wave breaking. To these ends, we construct two different graphical representations of the wave-breaking behavior of the system: a map of cutoff contours (Fig. 3) and a map of contours of maximum z_0 (Fig. 4).

A. Map of cutoff contours

The condition $\partial\xi/\partial z_0\leqslant 0$ implies that wave breaking will not occur if the minimum value of the derivative $\partial\xi/\partial z_0$ is positive. The "cutoff" for wave breaking may therefore be characterized by the equality $(\partial\xi/\partial z_0)_{\min}=0$, where the derivative is minimized with respect to both z_0 and τ. Since the solution for the function ξ is determined by the values of the system parameters, there exists a mapping F: $\Re^3\rightarrow\Re$ which takes the trio of real-valued parameters (E_m,β_b,η) into the value $(\partial\xi/\partial z_0)_{\min}$. The cutoff condition may then be written

$$\left(\frac{\partial\xi}{\partial z_0}\right)_{\min}=F(\eta,\beta_b,E_m)=0. \tag{12}$$

Equation (12) describes a surface that separates the trapping and nontrapping regions in a three-dimensional space of the parameters (E_m,β_b,η). Figure 3 shows contours of this surface in the plane of E_m and η, for several values of β_b. Individual points along these contours were obtained by numerically integrating Eq. (11), extrapolating the minimum value of the derivative $\partial\xi/\partial z_0$, and manipulating E_m and η so as to bring this minimal value within ± 0.001 tolerance of zero. In the limit of small amplitude waves, $E_m\rightarrow 0$, and the cutoff curves approach a common intercept at $\eta=0.5$, indicating that wave breaking always occurs (to some degree) if

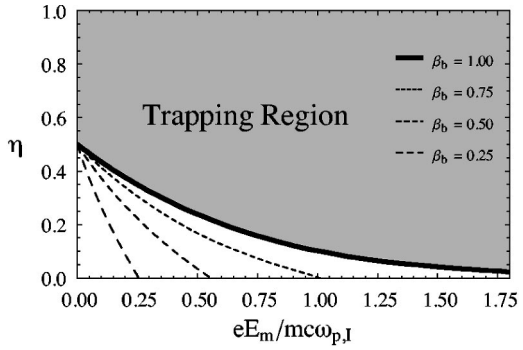

FIG. 3. Contours of $(\partial\xi/\partial z_0)_{\min}=0$ for different values of β_b (1.00, 0.75, 0.5, and 0.25). Wave breaking occurs in the upper right region of the curve corresponding to the given value of β_b. In the limit of small amplitudes, the cutoff occurs at $\eta=0.5$.

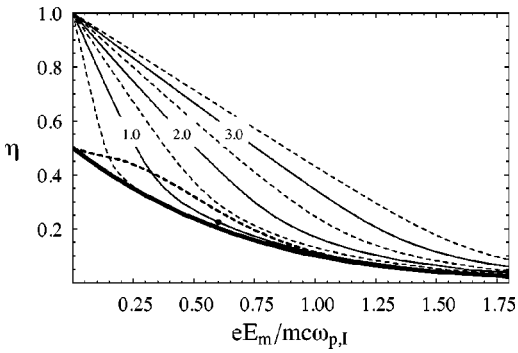

FIG. 4. Contours of constant $\hat{z}_0$ are shown as thin solid curves labeled by the corresponding integer values of $k_{p,\mathrm{I}}\hat{z}_0$. Intermediate curves corresponding to half-integer values of $k_{p,\mathrm{I}}\hat{z}_0$ are dashed and unlabeled. These contours lie above the cutoff (heavy solid curve). The contour for $\check{z}_0=0$ is superimposed on the figure as a heavy dashed curve. The point in parameter space corresponding to the graphs of Fig. 5 is marked by a dot that lies on the $k_{p,\mathrm{I}}\hat{z}_0=1$ contour.

the ion density decreases by a factor of more than one half between regions I and II. The intercepts along the horizontal axis, representing the values of E_m at which wave breaking occurs in a plasma of uniform ion density, are in agreement with the values predicted by setting $\beta_m=\beta_b$ in Eq. (6). The values of z_0 which minimize the derivative in Eq. (12) are found to lie approximately in the region between $k_{p,\mathrm{I}}z_0=0$ (at small amplitudes) and $k_{p,\mathrm{I}}\approx 0.5$ (at large amplitudes). Consequently, for points in parameter space which lie sufficiently close to the cutoff contour, a small downstream region of initial particles, beginning at $z_0=0$, are excluded from the wave breaking. We will return to this point below.

B. Map of contours of constant z_0

Consider that $\partial\xi/\partial z_0$ is a function of the variables z_0 and τ. For points in parameter space inside the trapping region, there exists a region R in the first quadrant of the z_0-τ plane on which the condition $\partial\xi/\partial z_0\leqslant 0$ is satisfied (since wave breaking occurs after the beam crosses the boundary and only particles initially located downstream participate in wave breaking). Let C be the closed curve bounding the region R, and let $(\hat{z}_0,\hat{\tau}),(\check{z}_0,\check{\tau})\in C$ denote the points where z_0 takes its maximum and minimum values, $\hat{z}_0$ and $\check{z}_0$, respectively, along the curve C.

Physically, $\hat{z}_0$ represents the downstream extent of the initial region of plasma which becomes involved in wave breaking. Its value varies according to the choice of parameter values. Let G denote the mapping G: $\Re^2\rightarrow\Re$ which takes the pair of real-valued parameters (E_m,η) into the corresponding value of $\hat{z}_0$. We eliminate the parameter β_b by restricting ourselves to the ultrarelativistic limit $\beta_b=1$. The resulting equation,

$$\hat{z}_0=G(E_m,\eta), \tag{13}$$

defines a surface in the three-dimensional space $(E_m,\eta,\hat{z}_0)$. Figure 4 shows contours of this surface in the plane of E_m and η, for several values of $\hat{z}_0$, which are normalized to the upstream plasma skin depth $k_{p,\mathrm{I}}^{-1}$. The problem of finding the values of the parameters (E_m,η) corresponding to a particular $\hat{z}_0$ is resolved by noting that the curve C mentioned previously is the set of points (z_0,τ) along which $\partial\xi/\partial z_0=0$, and that the points $(\hat{z}_0,\hat{\tau})$ and $(\check{z}_0,\check{\tau})$ are the intersections of C with the curve defined by $\partial^2\xi/\partial\tau\partial z_0=0$. Consequently, we can determine the value $\hat{z}_0$ for a set of parameter values corresponding to a point in the trapping region of Fig. 4 by integrating Eq. (11), and then adjusting the values (E_m,η) so as to bring the minimal value of $\partial\xi/\partial z_0$, plotted as a function of τ at constant $z_0=\hat{z}_0$, to within a ± 0.001 tolerance of zero. The resulting contours of constant $\hat{z}_0$ shown in Fig. 4 are found to lie above the heavy cutoff contour transposed from Fig. 3 and to intersect the vertical axis at $\eta=1$.

The value of $\hat{z}_0$ labeling the contour that passes through a given point (E_m,η) in the trapping region of parameter space denotes the downstream extent of initial wave-breaking particles for those values of the parameters. However, it is the difference between the maximal and minimal values $\Delta z_0\equiv\hat{z}_0-\check{z}_0$ which represents the length of the downstream interval of plasma that participates in wave breaking, and therefore it is this quantity that measures the number of wave-breaking particles, given by $N=\lambda_{0,\mathrm{II}}\Delta z_0$, where $\lambda_{0,\mathrm{II}}$ is the linear electron density in the downstream region prior to the passage of the beam. In terms of our dimensionless parameters, we may express the fractional quantity

$$f=(1-\eta)k_{p,\mathrm{I}}\Delta z_0, \tag{14}$$

which represents the ratio of the number N of wave-breaking particles to the initial number of particles in the upstream region per plasma skin depth $f\equiv Nk_{p,\mathrm{I}}/\lambda_{0,\mathrm{I}}$.

Repeating for various values of $\check{z}_0$ the procedure outlined above for plotting the curves in Fig. 4, would produce a second map, one of contours of constant minimum z_0. The $\check{z}_0=0$ curve from this hypothetical map has been superimposed upon the $\hat{z}_0$ contours in Fig. 4, where it appears as a heavy dashed line. This curve, which actually represents the inner edge of a $\check{z}_0=0$ plateau, does not coincide with the heavy cutoff contour transposed from Fig. 3, but rather turns out into the trapping region, dividing it into two subregions. For points in parameter space lying in the region above the $\check{z}_0=0$ curve, $\Delta z_0\equiv\hat{z}_0$, and Eq. (14) can be written $f=(1-\eta)k_{p,\mathrm{I}}\hat{z}_0$.

For points lying in the region between the cutoff curve and the $\check{z}_0=0$ curve, $\check{z}_0$ takes various values between zero and approximately one half of a plasma skin depth. This region of nonzero values for $\check{z}_0$ is of particular interest, because it implies that a small interval of initial particles near the boundary is excluded from the wave breaking. The dot on the $k_{p,\mathrm{I}}\hat{z}_0=1$ contour in Fig. 4 marks a point in this region. Figure 5 shows the evolution of wave breaking for the choice of parameters corresponding to this point, including a shaded area highlighting the expanding interval of initial particles involved in wave breaking. The lack of shading in the region extending from zero to $k_{p,\mathrm{I}}\check{z}_0=0.1003$ illustrates the predicted initial interval of excluded particles. These may be interpreted as particles that are so close to the interface that

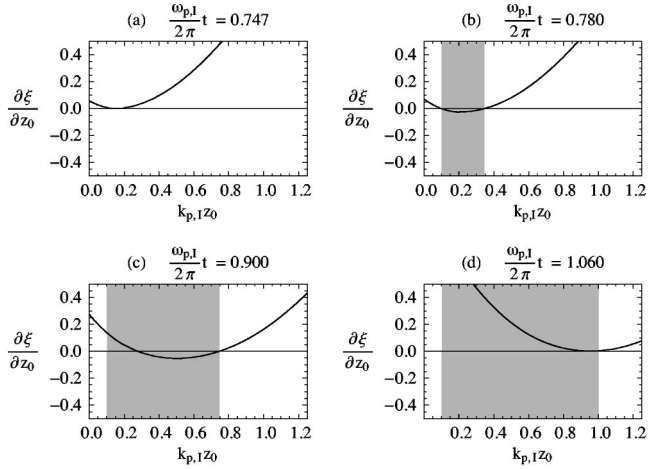

FIG. 5. Plots of $\partial\xi/\partial z_0$ at four different times for a choice of parameters ($\eta=0.225$, $eE_m/mc\omega_{p,I}=0.6$) which lie inside the wave-breaking region show (a) wave breaking beginning at a point just downstream of the discontinuity, (b) an interval of plasma (shaded region) becoming involved in wave breaking and (c) traveling downstream until (d) at $k_{p,I}z_0=1$ the wave breaking ends.

their sojourn in region II prior to crossing the interface is too brief for them to be rephased sufficiently to become involved in the wave breaking.

V. PARTICLE-IN-CELL SIMULATIONS

The Lagrangian fluid model described above provides the following predictions about the wave-breaking behavior of a plasma wave crossing a density transition.

(1) Wave breaking occurs for values of the parameters E_m and η which lie in the shaded region of Fig. 3, and specifically for $\eta>0.5$.

(2) For choices of parameters lying in the region of trapping space bounded by the $\check{z}_0=0$ contour and the trapping cutoff curve in Fig. 4, a small downstream region of initial particles does not participate in wave breaking.

(3) The fractional number of wave-breaking particles is given by Eq. (14).

In order to determine to what extent these statements about wave breaking are relevant to trapping behavior, a series of one-dimensional particle-in-cell (PIC) simulations was performed. The simulation results were found to be in good agreement with the Lagrangian fluid model up to the point of wave breaking. Wave breaking is found in both cases to be initiated on the upstream (higher density) side of the interface. The agreement between the PIC and fluid model is illustrated in Fig. 6, which shows snapshots of the longitudinal electric field and the plasma phase space at the onset of wave breaking. Figure 7 shows the longitudinal PIC phase space of the plasma after trapping has occurred. A rectangular box has been drawn to highlight the trapped particles trailing the first peak in fluid velocity. Their separation in momentum from the rest of the fluid demonstrates the acceleration mechanism provided by the field gradients in the plasma wave.

For the purpose of comparing the numbers of trapped versus wave-breaking particles, a series of PIC simulations was conducted in which the initial upstream plasma density and field amplitude were fixed at the values $n_{0,I}=5.833\times10^{13}$ cm^{-3} and $eE_m/mc\omega_{p,I}=0.5$, while the downstream density was manipulated to produce different values of η. The number of macroparticles trapped due to the wave breaking produced by the first peak of the plasma wave was extracted from the computed phase space coordinates, and the ratio f of trapped particles to the initial number of upstream particles per plasma skin depth was calculated. These results were then compared with a sampling of the parameter space of Fig. 3 along a vertical path located at $eE_m/mc\omega_{p,I}=0.5$. Figure 8 shows the number of wave-breaking particles predicted by the fluid model (triangles) alongside the number of trapped particles extracted from the PIC simulations (squares), for various values of η. Since these plots show good agreement on the value of η where wave breaking and trapping begin, the *threshold* for trapping is clearly identified. As η increases (i.e., the density transition becomes more pronounced), both the number of wave-breaking particles from the fluid analysis and the number of trapped particles from the PIC simulations increase initially and then asymptote to some constant value. However, the number of trapped particles rises to only approximately one half of the number of particles which participate in wave breaking. This discrepancy illustrates an important clarification provided by the PIC simulations: the initial region of plasma which becomes trapped spans *both* sides of the den-

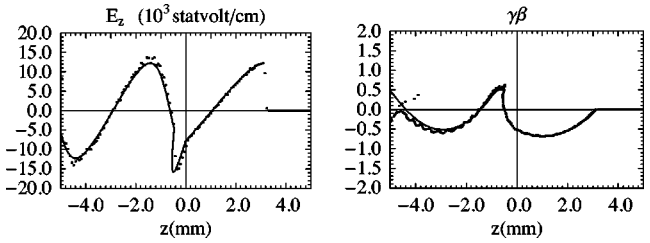

FIG. 6. Superimposed plots of electric field and normalized momentum, for the parameter values $\eta=0.4$, $eE_m/mc\omega_{p,I}=0.5$, show good agreement between the fluid model (solid curves) and the PIC simulation (dots) at the onset of wave breaking.

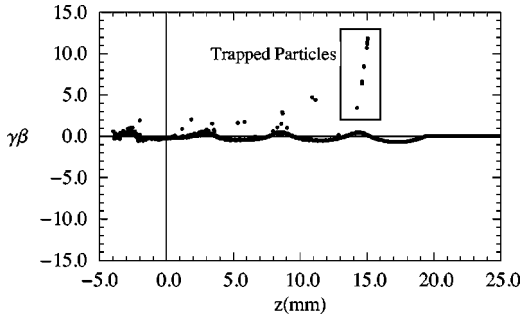

FIG. 7. A phase space plot from a 1D PIC simulation 64 ps after the beam has crossed the density transition with the parameter values $\eta=0.375$ and $eE_m/mc\omega_{p,I}=0.5$ illustrates the trapping of background plasma particles (contained inside the box) by the plasma wave.

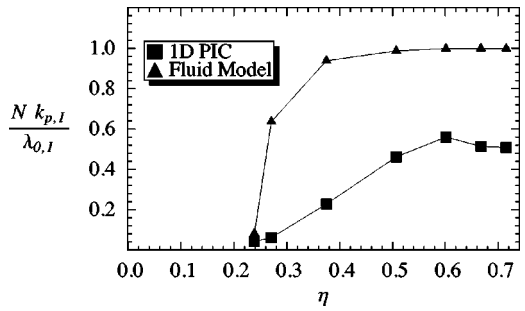

FIG. 8. These plots, at an electric field amplitude of $eE_m/mc\omega_{p,I}=0.5$, illustrate the discrepancy between the numbers of wave-breaking particles from the fluid model (triangles) versus trapped particles from the 1D PIC simulations (squares), but show good agreement in the value of η where trapping begins and similar asymptotic behaviors at large η. The vertical axis is the number of particles expressed as a fraction of the number of initial upstream particles per plasma skin depth.

sity transition. By contrast, the fluid analysis predicts that only particles on the downstream (lower density) side of the interface participate in wave breaking. In the fluid analysis, the asymptotic behavior in Fig. 8 arises from a cancelling effect between the increasing region of plasma involved in wave breaking and a decrease in the downstream density as η is increased, while in the PIC trapping simulations it is due to a falloff in the number of new upstream particles successfully injected into the plasma wave with each increase in the value of η.

Thus the comparison of the fluid and PIC analyses clearly shows that while wave breaking is a necessary condition for trapping, the fluid analysis does not successfully predict which particles are trapped after the wave-breaking condition is satisfied. In hindsight this is not surprising because the fluid treatment loses its rigorous validity after wave breaking, and there is therefore no reason to expect that a parameter such as the trapped population would be calculated correctly. Nevertheless, the Lagrangian fluid analysis has allowed a critical step forward in that we may predict exactly the threshold in parameter space where trapping begins.

VI. CONDITIONS FOR APPLICABILITY OF THE RESULTS

A note should be made regarding the assumptions of the preceding analysis and the restrictions which these assumptions impose upon the physical system. In particular, our invocation of the one-dimensional limit and our treatment of the beam as a δ function in z require that the transverse and longitudinal dimensions σ_r and σ_z be large and small, respectively, compared to a plasma skin depth, or

$$k_p\sigma_z \ll 1, \quad k_p\sigma_r \gg 1. \tag{15}$$

The requirement $k_p\sigma_r \gg 1$ arises from the need to avoid a large transverse electric field in the plasma, with its concomitant transverse plasma electron motion. This criterion is developed straightforwardly with the bounds of validity of linear theory. However, for cases of interest, linear theory, which does not self-consistently take into account the effects of the beam magnetic field on the plasma electron motion, may not serve as a guide. Recent work by Barov, Rosenzweig, and Thompson [7] has in fact extended the results of linear theory in the case of a disk-shaped beam with a δ-function distribution in z. In this analysis it was found that, even for beams of very large charge where the plasma response is nonlinear, the longitudinal electric field immediately behind the beam is *identical* to that predicted by linear theory. In addition, the combination of plasma electron transverse motion due to the beam's radial electric field and redirection of the motion by the beam's azimuthal magnetic field produces a strong longitudinal momentum kick forward. This kick, similar to the ponderomotive kick forward due to an ultrashort laser pulse, as in the LWFA case mentioned above, is not uniform, but has a radial dependence that limits its effect to a region within a plasma skin depth of the beam's radial edge. Consequently, in the case of a beam of large but finite radius and zero length, the excitation experienced by plasma electrons lying along the path of the beam and well within the beam's radius consists primarily of a transient backward impulse produced by the longitudinal electric field behind the beam.

However, Barov, Rosenzweig, and Thompson find that the predictions of the linear 2D analysis deviate from the results of 2D particle-in-cell simulations for a beam of finite length ($k_p\sigma_z=1.1$) as the beam charge is permitted to greatly exceed the charge of plasma electrons in a cubic skin depth. This indicates that the bounds of validity for a one-dimensional approximation in the case of a wide beam of small but nonzero length are additionally restricted by an upper limit on the beam density. A qualitative assessment of the findings of Ref. [7] suggests that in order for the one-dimensional limit to apply under the conditions of Eq. (15), the beam density should not greatly exceed the ambient density of the plasma. However, a comprehensive understanding of the extent to which wave breaking of the sort described under the simplifying assumptions of our 1D model contributes to trapping in a fully nonlinear three-dimensional system must await additional efforts in the form of higher-dimensional (2D and 3D) particle-in-cell simulations, and extensions to the 2D theory. In this respect, the present discussions are intended as a prelude to more extensive future work.

VII. CONCLUSIONS

We have, in the above analysis, employed a fully relativistic Lagrangian fluid model to examine the phenomenon of wave breaking due to a density transition in a 1D plasma wave of relativistic phase velocity. This analysis has produced some exact results that have clarified the wave-breaking process, allowing us to identify which Lagrangian fluid elements engage in wave breaking, where this wave breaking occurs, and most importantly, which combinations of plasma and wave parameters produce wave breaking. The present analysis stands in contrast to the Eulerian picture previously developed in Ref. [1]. This contrasting view is related to the shift of viewpoint from the Hamiltonian analy-

sis of electron motion in an approximate assumed potential, where one is concerned with *trapping*, which must be distinguished from the concept of *wave breaking*, or the breakdown of the fluid assumption.

As neither the Eulerian-Hamiltonian analysis of Ref. [1], nor the present Lagrangian model can answer in detail the question of how wave breaking and trapping are connected, one-dimensional particle-in-cell simulations were performed to provide a basis for comparison. These numerical studies indicate that the fluid model provides a good description of a 1D plasma wave up to the point of wave breaking, and that it correctly predicts the parameter values where trapping is initiated. The PIC simulations indicate that the results of the fluid analysis cannot, however, be reliably extended past the onset of wave breaking. In particular, the magnitude of the interval of initial fluid elements which participate in the wave-breaking process is found to be a poor predictor of the number of trapped particles (Fig. 8). The PIC simulations also reveal that particles on the upstream side of the density transition may become trapped in the plasma wave. A more detailed study of the mechanism by which these particles become trapped will be the subject of a future paper.

ACKNOWLEDGMENTS

The authors would like to thank H. Suk, M. Thompson, E. Esarey, and S. Cowley for helpful discussions. This work was supported by the U.S. Department of Energy under Grant No. DE-FG03-92ER40693.

[1] H. Suk, N. Barov, and J. B. Rosenzweig, Phys. Rev. Lett. **86**, 1011 (2001).

[2] C. E. Clayton, K. A. Marsh, A. Dyson, M. Everett, A. Lal, W. P. Leemans, R. Williams, and C. Joshi, Phys. Rev. Lett. **70**, 37 (1993).

[3] K. Nakajima, D. Fisher, T. Kawakubo, H. Nakanishi, A. Ogata, Y. Kato, Y. Kitagawa, R. Kodama, K. Mima, H. Shiraga, K. Suzuki, K. Yamakawa, T. Zhang, Y. Sakawa, T. Shoji, Y. Nishida, N. Yugami, M. Downer, and T. Tajima, Phys. Rev. Lett. **74**, 4428 (1995).

[4] C. W. Siders, Phys. Rev. Lett. **76**, 3570 (1996).

[5] F. Amiranoff, S. Baton, D. Bernard, B. Cros, D. Descamps, F. Dorhies, F. Jacquet, V. Malka, J. R. Marqués, G. Mathieussent, P. Miné, A. Modena, P. Mora, J. Morillo, and Z. Najmudin, Phys. Rev. Lett. **81**, 995 (1999).

[6] A. I. Akhiezer and R. V. Polovin, Sov. Phys. JETP **3**, 696 (1956).

[7] N. Barov, J. B. Rosenzweig, and M. C. Thompson, Phys. Rev. Lett. (to be published).